How to cite: *Angew. Chem. Int. Ed.* **2025**, *64*, e202421936
doi.org/10.1002/anie.202421936

Biosensing **Hot Paper**

A Small-Molecule Approach Enables RNA Aptamers to Function as Sensors for Reactive Inorganic Targets

*Tushar Aggarwal[+], Liming Wang[+], Bryan Gutierrez, Hakan Guven, Huseyin Erguven, Sarah Cho, and Enver Cagri Izgu**

Abstract: Fluorescent light-up aptamer (FLAP) systems are promising (bio)sensing platforms that are genetically encodable. However, FLAP-mediated detection of each distinct target necessitates either in vitro selection or engineering of nucleic acid sequences. Furthermore, an aptamer that binds an inorganic target or a chemical species with a short lifetime is challenging to realize. Here, we describe a small-molecule approach that makes it possible for a single FLAP system to detect chemically unique, non-fluorogenic, and reactive inorganics. We developed functionalized pre-ligands of RNA aptamers that bind benzylidene imidazolinones (Baby Spinach, Broccolli, Squash). Reactive inorganics, hydrogen sulfide (H_2S/HS^-) and hydrogen peroxide (H_2O_2), can specifically convert these pre-ligands into native ligands that fluoresce with FLAPs. Adaptation of this platform to live cells opened an opportunity for constructing whole-cell sensors: *Escherichia coli* transformed with a Baby Spinach-encoding plasmid and incubated with pre-ligands generated fluorescence in response to exogenous H_2S/HS^- or H_2O_2. Leveraging the functional group reactivity of small molecules eliminates the requirement of in vitro selection of a new aptamer sequence or oligonucleotide scaffold engineering for distinct molecular targets. Our method allows for detecting inorganic, short-lived species, thereby advancing FLAP systems beyond their current capabilities.

Introduction

Aptamers are structured nucleic acid sequences that selectively bind a (bio)chemical target with high affinity.[1,2] Aptamer sequences can be found in nature as gene regulation elements located in the untranslated regions of mRNAs,[3] or discovered in the laboratory by in vitro selection (or systematic evolution of ligands by exponential enrichment, SELEX) from a pool of nucleic acids.[4] Some in vitro-selected aptamers can bind and increase the fluorescence quantum yield (Φ_F) of fluorogenic small-molecule ligands that are otherwise poorly fluorescent in their unbound state.[5] These aptamers, called fluorescent light-up aptamers (FLAPs) or fluorogenic aptamers, can serve as genetically encodable and biocompatible sensing platforms. FLAP systems have attracted significant attention across several areas, including environmental monitoring,[6] forensics,[7] bioanalyte detection and clinical diagnostics,[8–12] live cell imaging,[13–17] and synthetic biology.[18,19]

In principle, a FLAP consensus region that specifically binds an organic molecule ligand (Figure 1A) has no direct utility for detecting an inorganic target (Figure 1B). Further, the aptamer ligand must have intrinsic fluorogenicity to generate a signal with FLAPs, which renders non-fluorescent chemical species unsuitable for detection. Recent aptamer-based sensors that detect non-fluorescent targets have employed a secondary aptamer domain that binds the target to induce folding and/or conformational stabilization of a tethered FLAP.[13,20,21] Though elegant in design, the target-binding aptamer domain must be in vitro selected or engineered for each target of interest. Additionally, programming complex RNA scaffolds that correctly and conditionally fold can be difficult due, in part, to the highly dynamic interactions among long RNA transcripts[22,23] and inherent limitations in RNA stability or folding under suboptimal physiological conditions.[24] Finally, the aptamer-ligand binding is an equilibrium process that relies on the local availability of free ligands.[25] As a result, it would be challenging to realize an aptamer system that can bind targets with limited chemical or biological lifetime.

Here, we describe a structure- and reactivity-guided small-molecule approach that can help address these

[*] Dr. T. Aggarwal,[+] L. Wang,[+] Dr. B. Gutierrez, H. Guven, Dr. H. Erguven, S. Cho, Prof. Dr. E. C. Izgu
Department of Chemistry and Chemical Biology
Rutgers University
New Brunswick, NJ-08854, USA
E-mail: ec.izgu@rutgers.edu
Prof. Dr. E. C. Izgu
Cancer Institute of New Jersey
Rutgers University
New Brunswick, NJ-08901, USA
Prof. Dr. E. C. Izgu
Rutgers Center for Lipid Research, New Jersey Institute for Food, Nutrition, and Health
Rutgers University
New Brunswick, NJ-08901, USA
[+] These authors contributed equally to this work

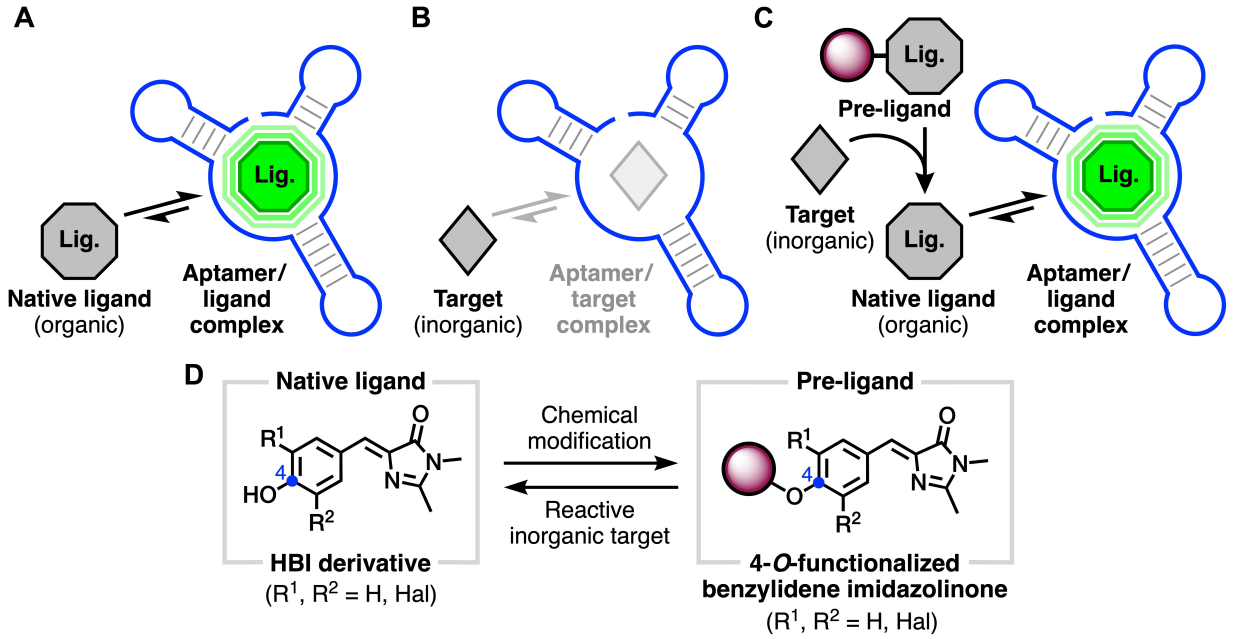

Figure 1. Conceptual illustration of how a FLAP system can be repurposed to detect an inorganic molecular target without aptamer engineering. (A) Strong fluorescence induced by non-covalent binding interactions between an aptamer and its native, intrinsically fluorogenic ligand. (B) Inorganic targets, like majority of biologically relevant molecules, may lack fluorogenicity, affinity for a structured nucleic acid, or both. (C) If exists, the chemical reactivity of the inorganic target can be utilized to form the native aptamer ligand in situ from a pre-ligand that has a reduced fluorogenic binding. This would allow for the detection of inorganic targets by a single FLAP system, thereby expanding the application space of structured nucleic acids without in vitro selection or additional oligonucleotide scaffold engineering. (D) Interconversion between an aptamer ligand [e.g., 4-hydroxybenzylidene imidazolinone (HBI) derivative] and pre-ligand (e.g., 4-*O*-functionalized-benzylidene imidazolinone).

fundamental challenges. This approach allows for a single aptamer known to bind one class of organic fluorogens to detect multiple, structurally unique, non-fluorogenic, and reactive inorganics (Figure 1C). The RNA aptamer Spinach binds 4-hydroxybenzylidene imidazolinone (HBI) and its analogs with a K_d in the nanomolar to micromolar range.[26–28] Guided by molecular docking calculations and functional group reactivity principles in synthetic organic chemistry, we developed 4-*O*-functionalized benzylidene imidazolinone architectures that exhibit weak or inhibited fluorescent binding toward Baby Spinach (Figure 1D). The RNA aptamer Baby Spinach (51-nt)[27] is a truncated version of Spinach2 (95-nt).[29] The 4-*O*-functionalized benzylidene imidazolinones, referred to as "pre-ligands", can be converted into native HBIs (4-*O*H) by an inorganic target. This study focused on redox-active inorganics with major biochemical roles and short physiological half-lives: hydrogen sulfide (H_2S) and hydrogen peroxide (H_2O_2). H_2S is a reactive sulfur species (RSS) that acts as a reducing agent. It has cytoprotective properties against oxidative stress[30] and is involved in signaling that pertains to neurological[31–34] and cardiovascular[35,36] processes. H_2S can diffuse through lipid membranes without the aid of channels.[37] H_2O_2 is a reactive oxygen species (ROS) involved in various biological processes, ranging from signal transduction and cell differentiation to oncogene activity.[38–43] H_2O_2 transport across membranes occurs through simple diffusion or aquaporins in aerobic organisms.[44,45]

The activity-based sensing method using FLAPs and pre-ligands can detect H_2S/HS^- or H_2O_2 with good selectivity against other redox species. Adaptation of this method to live cells through plasmid transfection opens a new opportunity for building whole-cell biosensors: *Escherichia coli* competent cells (BL21-DE3) transformed with a Baby Spinach-encoding plasmid and incubated with the selected pre-ligand fluoresce in response to H_2S/HS^- or H_2O_2. Whether in cell-free conditions or with *E. coli*, implementing the FLAP/pre-ligand system avoids nucleic acid scaffold engineering or in vitro selection of a new aptamer consensus sequence. Further, this approach makes it possible to detect chemical species traditionally not considered aptamer targets (or ligands) due to their intrinsic reactivity or lack of nucleic acid binding interactions. Our method leverages the functional group reactivity of small molecules to build cell-based sensors for chemically distinct targets, which exploits a previously overlooked synergism between synthetic organic chemistry and synthetic biology.

Results and Discussion

Docking Calculations aid in Experimental Interpretation and Guide Aptamer pre-Ligand Design

To structurally rationalize the effect of ligand functionalization on aptamer binding, we performed molecular docking (Figures 2 and S1) using AutoDock Vina 1.2.0,[46,47] which

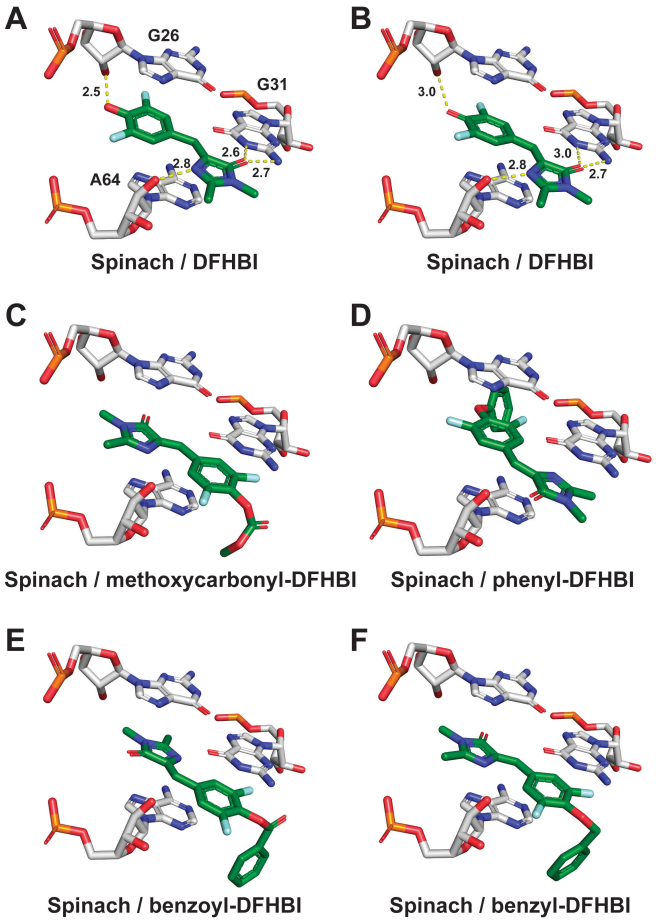

Figure 2. Docked poses: binding mode of the selected 4-*O*-aryl-modified derivatives of DFHBI. (A) Model of key hydrogen-bonding interactions within the crystal structure of Spinach-DFHBI (PDB:4TS2) near the binding site. (B) Binding mode of DFHBI docked using AutoDock Vina. (C–F) docked poses of the 4-*O*-aryl-modified small molecule derivatives of DFHBI.

presents a success rate of >90 % in detecting receptor-ligand bindings with an average RMSD of <2.0 Å.[48] Recognizing the limitation of Auto-dock Vina in terms of modeling heteroatoms, we used methoxycarbonyl, phenyl, benzyl, and benzoyl substituents to mimic more complex 4-*O*-functional groups that we envisioned to synthetically incorporate into benzylidene imidazolinone. The initial simulations used DFHBI due to the availability of Spinach/DFHBI co-crystal structure.[27] Docking results with additional benzylidene architectures are presented in Figures S1 and S2. Based on the crystal structure,[27] DFHBI has a near-planar geometry and forms key hydrogen bonding interactions with G26, G31, and A64 nucleobases of Spinach (Figure 2A). These interactions were largely retained, with similar hydrogen bond lengths in our docking simulation with DFHBI (Figure 2B, docking score of $-8.9\,kcal\,mol^{-1}$). This result validated that the native ligand-aptamer binding interactions can be attained *in silico* using AutoDock Vina. Strikingly, DFHBI molecules that are 4-*O*-functionalized with methoxycarbonyl, phenyl, benzoyl, or benzyl group bound G26/G31/A64 pocket with a near 180° rotation. In particular, the 4-*O*-benzylidene motif was positioned opposite to G26 for methoxycarbonyl-DFHBI (Figure 2C), benzoyl-DFHBI (Figure 2E), and benzyl DFHBI (Figure 2F). In the case for phenyl-DFHBI, the imidazolinone carbonyl was positioned opposite to G31 (Figures 2D). For all these benzylidene imidazolinone models, the native hydrogen-bonding interactions within the G26/G31/A64 pocket were abolished and the docking scores (methoxycarbonyl-DFHBI: −5.6, phenyl-DFHBI: 2.7, benzoyl-DFHBI: −5.6, and benzyl-DFHBI: $-6.6\,kcal\,mol^{-1}$) indicated significantly weaker binding affinity. Taken together, the docking results provided support for a scenario in which the positioning of the benzylidene imidazolinone motif within the G26/G31/A64 binding pocket of Spinach can be altered by functionalizing the 4-*O*-benzylidene atom as a carboxyl, ether, or an ester group.

Building the FLAP pre-Ligand Library

Redox-mediated chemical transformations of functional groups have been successfully implemented to release phenols.[49–52] Inspired by these transformations, and guided by our molecular docking simulations, we developed a library of benzylidene imidazolinones to serve as FLAP pre-ligands (Figure 3A). This library included compounds that we synthesized from various HBI derivatives to specifically react with either H_2S/HS^- (Figure 3A, left panel) or H_2O_2 (Figure 3A, right panel). See Supporting Information for details on their chemical syntheses. The H_2S/HS^--reactive designs included **a**zido**e**thyl**c**arbonyl-modified MFHBI (AEC-MFHBI) and DFHBI (AEC-DFHBI); **di**nitro**p**henyl-modified MFHBI (DNP-MFHBI); **p**yridyl**di**sulfunyl**benzoyl**-modified MFHBI (PyDSBz-MFHBI) and DBrHBI (PyDSBz-DBrHBI). The H_2O_2-reactive designs included 4-(**m**ethyl)**b**enzene**b**oronic **a**cid **p**inacol **e**ster-modified MFHBI (MBBAPE-MFHBI) and DFHBI (MBBAPE-DFHBI); and 4-(**m**ethyl)**b**enzene**b**oronic **a**cid-modified MFHBI (MBBA-MFHBI).

Among the pre-ligand candidates that would react with H_2S/HS^-, both AEC-MFHBI and AEC-DFHBI displayed poor selectivity against cysteine (Cys) and glutathione (GSH), which are nucleophilic thiols abundant in biological environments. We hypothesized that the conversion of these pre-ligands to MFHBI or DFHBI by Cys and GSH is through nucleophilic attack of thiol to the benzylidene carbonate. To test this hypothesis, we synthesized **m**ethoxy**c**arbonyl-MFHBI (MC–MFHBI) and subjected the mixture of MC–MFHBI and Baby Spinach to Cys, GSH, or H_2S separately (Figure S3). Signal-to-background ratios (F/F_0s) were calculated, where F and F_0 are the fluorescence intensities for samples with and without the redox species, respectively. Addition of Cys and GSH led to F/F_0 values of 18.5 and 3.5 for 2 hours of incubation, which are comparable to those for AEC-MFHBI (10.9 and 6.3). In contrast, the H_2S/HS^- treatment displayed less than 30 % fluorescence increase after 2 hours of incubation. These results indicate that (i) H_2S has weaker nucleophilic reactivity toward the benzylidene 4-*O*-carbonate than Cys and GSH, which is in agreement with previous reports,[53] and (ii) the conjugate

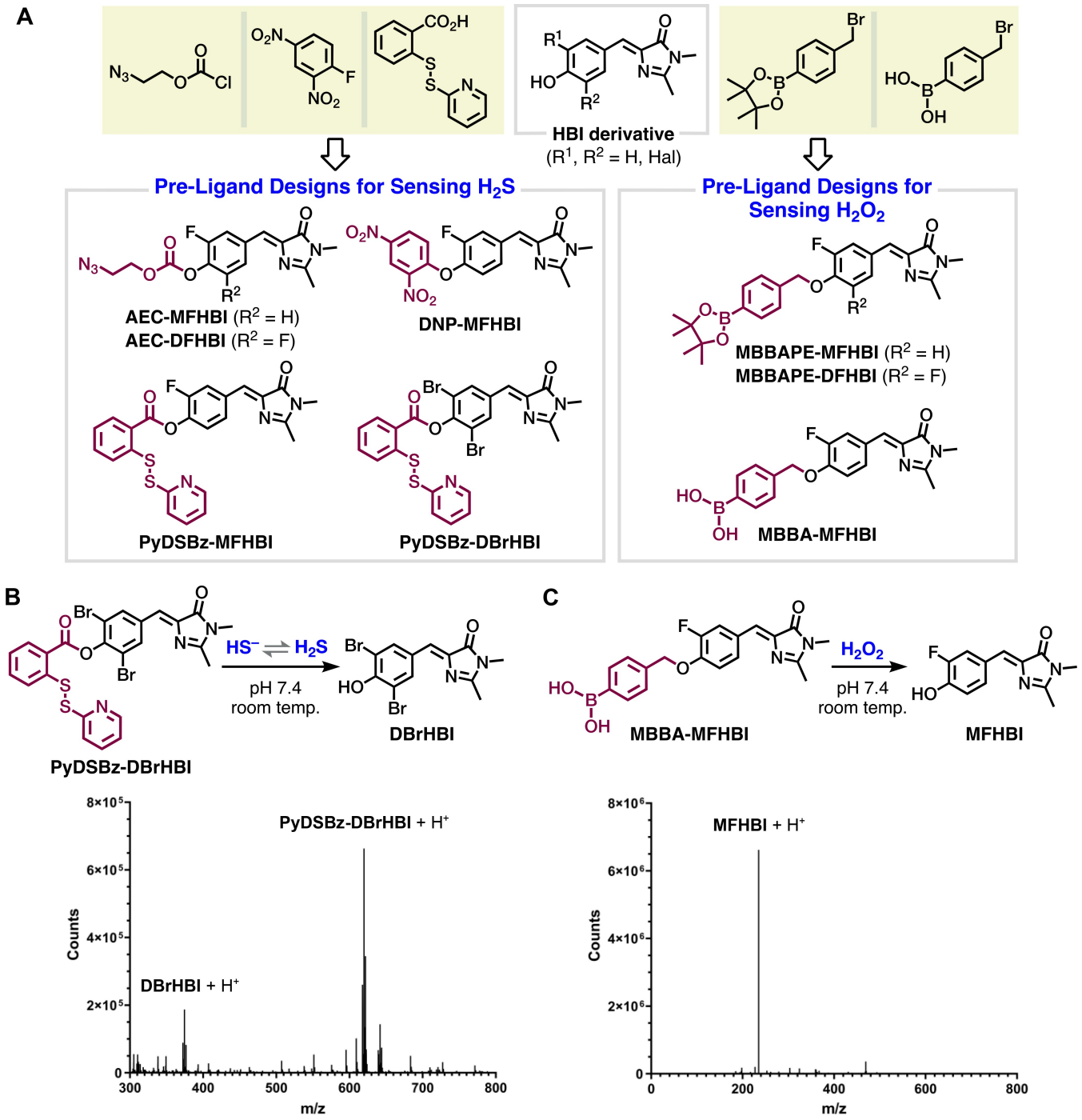

Figure 3. Baby Spinach pre-ligand designs and native ligand formation. (A) Pre-ligands synthesized from respective building blocks (yellow panels) for detecting (left) H_2S/HS^- or (right) H_2O_2. (B, top) Generation of DBrHBI from PyDSBz-DBrHBI by Na_2S treatment. (Bottom) Overlay of extracted mass spectrum acquired following liquid chromatography. For PyDSBz-DBrHBI, $[M+H]^+$ requires 619.9131; found 619.9116; for DBrHBI, $[M+H]^+$ requires 374.9162; found 374.9198. (C, top) Generation of MFHBI from MBBA-MFHBI by H_2O_2 treatment. (Bottom) Spectrum acquired via direct injection. For MFHBI, $[M+H]^+$ requires 235.0878; found 235.0922. No significant peak related to MBBA-MFHBI was observed. (B and C, bottom) Crude reaction aliquot was taken after 1 hour of mixing pre-ligand with the respective redox agent and analyzed in positive ionization mode. Peak heights are not an accurate representation of relative concentrations.

bases of MFHBI and DFHBI can serve as good leaving groups. Therefore, we reasoned that sterically blocking the benzylidene 4-*O*-carbonyl site would largely evade nucleophilic attack of thiols, thereby preventing non-specific signal generation while favoring H_2S-induced self-immolation.

This reasoning is conceptually supported by previous observations where sterically hindered esters showed in-

creased resistance against hydrolysis while favoring self-immolation.[54] Further, in the presence of Baby Spinach, both DNP-MFHBI and PyDSBz-MFHBI provided similar F/F_0 values for Cys and GSH. We presumed that the dinitrobenzyl moiety in DNP-MFHBI and the ester in PyDSBz-MFHBI may react with thiols. In this regard, incorporating a second fluorine atom on the benzylidene ring would render these probes even more reactive toward Cys and GSH. Therefore, we did not pursue the synthesis of their DFHBI analogs. Among the pre-ligands we have explored, PyDSBz-DBrHBI possesses a sterically hindered benzylidene 4-*O*-carbonyl, which in turn increases its selectivity toward H_2S/HS^-.

Among the pre-ligands designed to react with H_2O_2, both MBBAPE-MFHBI and MBBAPE-DFHBI displayed poor stability in near-neutral buffer. We observed their conversion to MFHBI and DFHBI prior to H_2O_2 treatment (high-resolution mass spectrometry, HRMS, analysis). Additionaly, their mixtures with Baby Spinach exhibited spontaneously increasing levels of fluorescence, suggesting that these DFHBI-derived compounds are too reactive to serve as pre-ligands. In contrast, MBBA-MFHBI is sufficiently stable in buffer. MBBA-DFHBI was not included into the pre-ligand library due to unresolved difficulties in its synthesis and isolation. In addition to these observations, our preliminary findings indicated that the aqueous solubility of boronic acid-containing pre-ligand design is superior to its boronic acid pinacol ester counterparts. All the pre-ligand designs we studied here, except for the MBBAPE analogs, are soluble in aqueous buffer (1 % v/v DMSO, pH 7.4) at concentrations reaching $\geq$100 μM. Based on all these evaluations, we therefore elected PyDSBz-DBrHBI and MBBA-MFHBI as FLAP pre-ligands for further experiments.

Importantly, docking of these pre-ligands to Spinach G26/G31/A64 pocket presented a similar degree of change in positioning (Figure S2). To dock MBBA-MFHBI, we substituted boron with CH for simulation compatibility. In both cases, the 4-*O*-benzylidene motifs were placed opposite to G26. The docking scores (PyDSBz-DBrHBI: −1.9, and dihydroxymethyl-MFHBI: −6.8 kcal mol^{-1}) indicated weaker binding affinity, which is consistent with the results obtained for the aformentioned generic functional groups (*cf.* Figures 2C–F).

Conversions of PyDSBz-DBrHBI and MBBA-MFHBI to their respective redox products, DBrHBI and MFHBI, were evaluated through HRMS (Figures 3B and 3C). For each pre-ligand design, we analyzed the crude reaction aliquot collected after 1 hour of mixing with the respective redox agent in physiologically relevant conditions. The spectral data indicated the presence of native ligand, DBrHBI or MFHBI, which validated the expected redox reactivity of benzylidene 4-*O*-modifications. Furthermore, we determined the benzylidene 4-O*H* pK_a of DBrHBI as 5.2 (Figure S4) and of MFHBI as 6.8 (Figure S5), indicating that these native ligands, once generated from PyDSBz-DBrHBI and MBBA-MFHBI, should exist primarily in their fluorescently enhanced anionic forms at physiological pH.

Binding Affinities of pre-Ligands Characterized by Fluorescence Quenching

We conducted a fluorescence quenching (competitive binding) assay to gain an understanding of the relative fluorogenic binding of these pre-ligands compared to their native counterparts (Figure 4A). To this end, we incubated Baby Spinach (1 μM) and its native ligand (2 μM) with varied concentrations of the pre-ligand and recorded fluorescence intensities after 60 minutes. The sample containing 50 μM of PyDSBz-DBrHBI exhibited a fluorescence intensity similar to that of 0 μM PyDSBz-DBrHBI, representing minimal competition between PyDSBz-DBrHBI and DBrHBI in binding Baby Spinach (Figure 4B). Incubation of Baby Spinach and MFHBI with 50 μM of MBBA-MFHBI, which is 25 equivalents of MFHBI, retained fluorescence intensity at ~70 % (Figure 4C). This observation indicates that the binding of MBBA-MFHBI to Baby Spinach may occur but

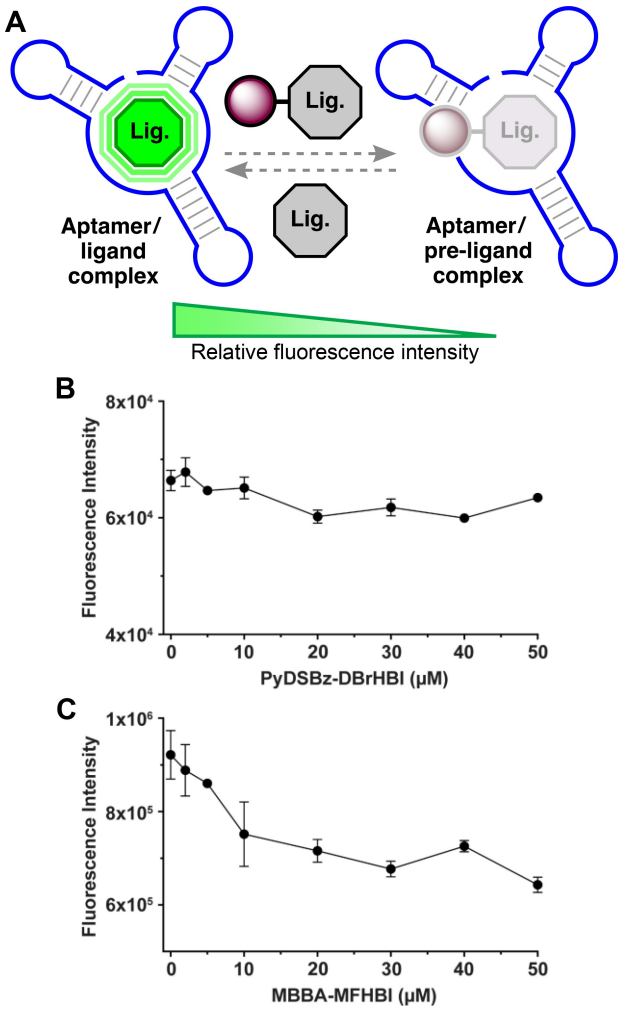

Figure 4. Fluorescence quenching with pre-ligands. (A) Aptamer affinities of pre-ligands were assessed via competitive ligand binding assay. Fluorescence intensities of (B) Baby Spinach/DBrHBI complex vs PyDSBz-DBrHBI concentration, and (C) Baby Spinach/MFHBI complex vs MBBA-MFHBI concentration. Error bars represent standard deviation, $n=3$.

is substantially weaker than the binding between MFHBI and Baby Spinach. Overall, these results correlate well with the disfavored binding of pre-ligands to Spinach as predicted from our docking calculations (*cf.* Figures 2E–F and S2).

Cell-Free Redox Sensing with FLAP/pre-Ligand Systems

The fluorescent signal generation rates, magnitudes, and selectivities of PyDSBz-DBrHBI and MBBA-MFHBI were evaluated via microplate reader measurements (Figure 5). The F/F_0 values for 60-minute incubation of the selected pre-ligand (5 μM) with Baby Spinach (1 μM) were calculated. Mammalian cells have been shown to respond to 10–600 μM of exogenous H_2S.[55]

In accordance, we reasoned that the addition of Na_2S at 500 μM into a pH 7.4 buffer could generate H_2S at a biologically relevant concentration (~100 μM). S^{2-} should be almost fully protonated to HS^- ($pK_a \geq 12.0$), and around 20 % of the sulfur species should exist in the form of H_2S (pK_a~7.0).[56] Therefore, the detection of HS^- correlates with the presence of H_2S.

Results for H_2S sensing indicated that Baby Spinach and PyDSBz-DBrHBI delivered ~3600 % increase in fluorescence intensity (486 vs 18,142) when incubated with Na_2S (500 μM) for 60 minutes compared to the untreated sample (Figures 5A). Fluorescence intensities of samples containing PyDSBz-DBrHBI plateaued at ~50 minutes and reached up to ~30 % of that with DBrHBI. To assess the performance of the H_2O_2-responsive pre-ligand, MBBA-MFHBI, we monitored the relative fluorescence intensity change of the Baby Spinach sample containing either MFHBI or MBBA-MFHBI in the presence of H_2O_2 (Figure 5D). After 60 minutes of the addition of H_2O_2 (100 μM) to the sample containing MBBA-MFHBI, we observed ~1800 % increase in fluorescence intensity (21,884 vs 414,252), compared to only 28 % increase without H_2O_2 addition. This result suggested that the phenyl boronic acid group of MBBA-MFHBI is stable at physiological pH and can generate free MFHBI upon reacting with H_2O_2. We confirmed the RNA aptamer backbone stability in the presence of H_2O_2 (100 μM) by denaturing PAGE analysis of Baby Spinach (Figure S6).

Next, we evaluated the redox specificities of pre-ligands PyDSBz-DBrHBI (Figure 5B) and MBBA-MFHBI (Figure 5E). The F/F_0 value for the control samples, which included only the pre-ligand and Baby Spinach in buffer ("untreated"), were set to 1 for comparison. For the mixture of Baby Spinach and PyDSBz-DBrHBI that was incubated with Na_2S (500 μM) for 60 minutes, F/F_0 was measured as 37.3. Importantly, when the same mixture was incubated with Cys or GSH, F/F_0 reached up to only 6.6 or 3.9, respectively. Other RSS we tested (SO_3^{2-}, $S_2O_3^{2-}$, SO_4^{2-}, and SCN^-) generated F/F_0 values centered around ~1, indicating

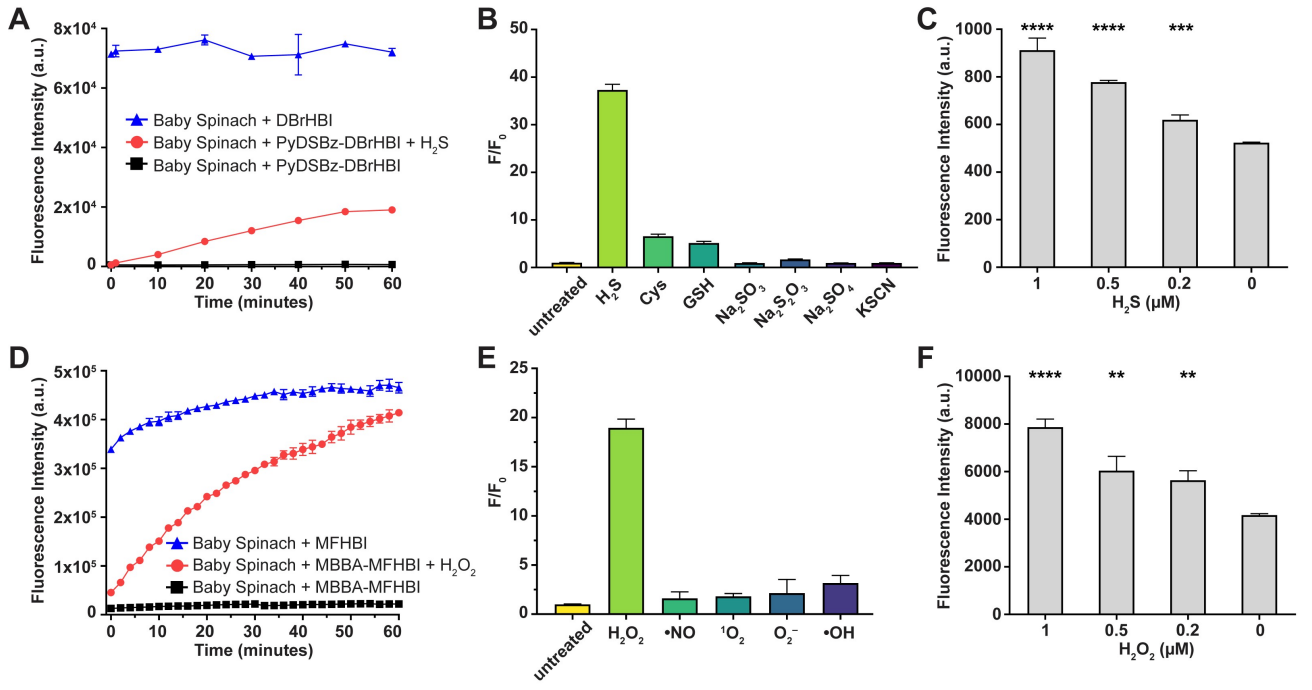

Figure 5. Performances of PyDSBz-DBrHBI and MBBA-MFHBI with Baby Spinach in cell-free conditions. (A, D) Time-dependent fluorescence increase of pre-ligands upon treatment with H_2S/HS^- (from Na_2S) or H_2O_2. (B, E) The fluorescence fold increase (F/F_0) measured 60 minutes after the addition of RSS (500 μM) and ROS (100 μM), respectively. Here, F and F_0 are the fluorescence intensities for samples with and without the redox species, respectively. (C, F) LoD measurements for Baby Spinach with PyDSBz-DBrHBI or MBBA-MFHBI incubated with H_2S/HS^- (from Na_2S) or H_2O_2 for 60 minutes. Conditions: DBrHBI, PyDSBz-DBrHBI, MFHBI, and MBBA-MFHBI (5 μM), Baby Spinach (1 μM), HEPES (pH 7.4, 50 mM), KCl (100 mM), $MgCl_2$ (10 mM), and Na_2S (500 μM) or H_2O_2 (100 μM). (A, B, and C) Data sets labeled as "H_2S" by convention. Single-tailed Student's t test: *, $P<0.05$; **, $P<0.01$; ***, $P<0.001$; ****, $P<0.0001$. Error bars represent standard deviation based on triplicates.

no measurable pre-ligand activation. As for the samples containing MBBA-MFHBI, F/F_0 was measured as 18.9 upon 60 minutes of incubation with H_2O_2 (100 μM). In contrast, F/F_0 values were <4 for other ROS, ($^{\bullet}NO$, $^1O_2$, $O_2^{-\bullet}$, $^{\bullet}OH$), suggesting that MBBA-MFHBI is selective for H_2O_2.

Limit of detection (LoD) values were determined for FLAP/pre-ligand systems by evaluating the statistical difference between F and F_0 measured at different concentrations of H_2S and H_2O_2, respectively (Figures 5C and 5F). Here, LoD is defined as the minimum redox species concentration at which F is statistically higher than F_0 ($P<0.05$) according to one-tailed Student's t test. We determined LoD for PyDSBz-DBrHBI as 0.2 μM of H_2S and that for MBBA-MFHBI as 0.2 μM of H_2O_2. The LoD of PyDSBz-DBrHBI is close to the other recently reported fluorescence-based H_2S/HS^- sensors.[57–59] The sensitivity of MBBA-MFHBI is comparable to fluorescence-based H_2O_2 sensors that use small-molecule fluorophore activation.[60,61] In addition to LoD, we evaluated the linear response range for the two FLAP systems. PyDSBz-DBrHBI with Baby Spinach responded to H_2S/HS^- linearly for the Na_2S concentration range of 10–200 μM (Figure S7A). The mixure of MBBA-MFHBI and Baby Spinach provided a linear response to 20–100 μM of H_2O_2 (Figure S7B).

To demonstrate that our pre-ligand design approach is broadly translatable as an RNA-based sensing platform, we used the pre-ligands PyDSBz-DBrHBI and MBBA-MFHBI with additional RNA aptamers. These assays involved Broccoli[62] and Squash,[63] which also bind HBI derivatives but differ in length and consensus sequence. With each of these RNAs, PyDSBz-DBrHBI and MBBA-MFHBI delivered a significant fluorescence increase upon treatment with Na_2S and H_2O_2, respectively (Figure S8). Furhermore, both pre-ligands exhibited weak aptamer binding based on fluorescence quenching (competitive binding) assays (Figures S9), indicating that 4-*O*-benzoylation and 4-*O*-benzylation can weaken the fluorogenic binding between the benzylidene imidazolinones and their cognate RNA aptamers. These results are consistent with those obtained for Baby Spinach (cf. Figures 4B–C) and suggest that our pre-ligand design approach is adaptable to other aptamers that use the same class of native ligands.

Turning E. coli Into Cell-Based Sensors using pET-21-3xBaby Spinach and pre-Ligands

Bacteria, notably *E. coli*, are convenient and robust model organisms widely employed for top-down construction of whole-cell biosensors.[64] In accordance, we focused on building chemically competent *E. coli* BL21 Star (DE3) cells as redox sensors, and initially transformed them with a DNA plasmid containing tRNA-Spinach2. Confocal imaging of *E. coli* with MFHBI (preliminary positive control) exhibited weak intracellular brightness following 488 nm excitation. Therefore, we designed and cloned a gene encoding for a tRNA fused with three continual Baby Spinach consensus regions, each connected through a 6-bp sealing stem, named pET-21-3xBaby Spinach (Figures 6A, S10, and S11). We reasoned that *E. coli* transcribing this pET-21-3xBaby Spinach construct would provide up to three ligand binding domains per transcript compared to tRNA-Spinach2 with a single binding domain, thus generate stronger fluorescence in the presence of native ligands. Indeed, we observed bright signals in samples incubated with DBrHBI (440 nm excitation, Figure 6B top-left, Figure 6C DBrHBI) or MFHBI (488 nm excitation, Figure 6D top-left, Figure 6E MFHBI). This observation supported the notion that RNA transcripts with multiple ligand-binding FLAP domains could amplify the fluorescence output, which is also in agreement with a previous report demonstrating an increase in brightness of Spinach-tagged guide RNA in CRISPR-Display.[65] In accordance, *E. coli* carrying pET-21-3xBaby Spinach plasmid (and grown in LB at 37 °C) were used for our subsequent experiments. RNA transcription was induced by the addition of 1 mM isopropyl β-D-1-thiogalactopyranoside once OD (600 nm) reached 0.4, and cells were grown for an additional 2 hours to further facilitate aptamer transcription. Harvested cells were incubated with M9 media containing either PyDSBz-DBrHBI (100 μM) or MBBA-MFHBI (100 μM) for 15 minutes. The media was replaced with fresh M9 media containing either H_2O_2 (100 μM) or Na_2S (2 mM). This media replacement ensured the removal of pre-ligand molecules not internalized by the cells. Although we have no direct measurement of intracellular concentrations of pre-ligands, we postulate that pre-ligands can be internalized by *E. coli* through passive diffusion while some may be secreted out through efflux. The signal generation could result from either passive diffusion of pre-ligands into *E. coli* followed by intracellular redox reaction or extracellular redox reaction of effluxed pre-ligands and subsequent cellular uptake. The latter mechanism, however, would constitute a major decrease in signal generation due to substantial dilution of pre-ligands when effluxed to the newly replaced media. Aliquots (1 mL) of *E. coli* culture were used at different time points for confocal imaging and a red membrane dye (Fm 4-64FX) was used as a co-stain to label the *E. coli* membrane. It is worth noting that the use of Fm 4-64FX allowed us to observe heterogeneity in the overall population for aptamer transcription levels, as the positive controls displayed different levels of brightness following excitation at either 440 nm or 488 nm (Figures 6B or 6D, top-left). Furthermore, it allowed for visualization of cell morphology from the time of pre-ligand addition until the end of redox incubation time. The observation that cells retained their morphology (rod shaped) indicated that *E. coli* tolerates the concentrations we used for pre-ligands (100 μM) and redox species (100 μM H_2O_2 or 2 mM Na_2S). Samples without DBrHBI (Figure 6B, top-middle) or MFHBI (Figure 6D, top-middle) served as a measure of background fluorescence while providing the microscopy parameters for subsequent confocal images and data analysis. *E. coli.* carrying the pUC19 plasmid (negative control), which lacks 3xBaby Spinach aptamer gene, exhibited no detectable fluorescence following 440 or 488 nm excitation in the presence of DBrHBI (Figure 6B, top-right) or MFHBI (Figure 6D, top-right), respectively.

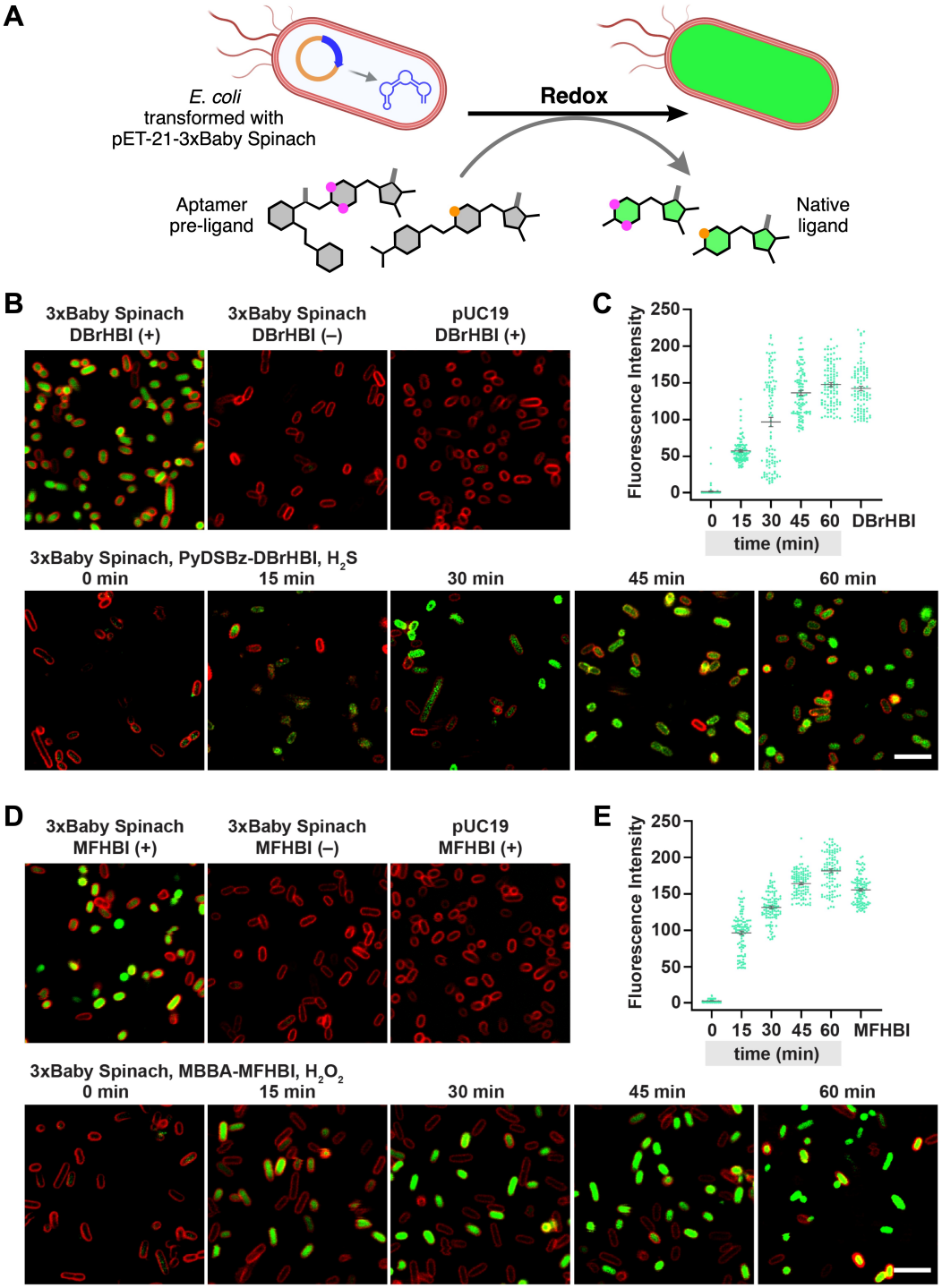

Figure 6. Turning *E. coli* into redox sensors. (A) When transformed with pET-21-3xBaby Spinach and incubated with a Baby Spinach pre-ligand, BL21 Star (DE3) *E. coli* can fluoresce in response to a redox cue. (B, D) Confocal microscopy images of live *E. coli* sensing (B) H_2S/HS^- or (D) H_2O_2. Top row panels represent positive and negative controls, including transfection with pUC19 plasmid, which contains no aptamer gene. Bottom row panels represent redox sensing at 0, 15, 30, 45, and 60 minutes. (C, E) Quantitative assessment of fluorescence outputs from cells over 60 minutes, along with the positive control measured at 60-minute time point using either (C) DBrHBI or (E) MFHBI. Cells were incubated in M9 media containing 100 μM of the HBI derivative. Redox species introduced to the imaging media: (B, C) H_2O_2 (100 μM), (D, E) Na_2S (2 mM). For co-staining, cells were treated with a FM 4-64FX (red membrane dye, 1 μg/ml, 2 minutes). Channel/excitation (nm): DBrHBI/440, MFHBI/488, Fm4-64FX/568. Scale bar: 5 μm. Error bars represent standard error of the mean.

We obtained the fluorescence intensity vs time plots (Figure 6C and 6E) from the confocal microscopy data by quantifying the mean fluorescence of each cell imaged at various time intervals from 0 (pre-treatment) to 60 minutes

(see Supporting Information for detailed procedure). This analysis allowed us to gain a quantitative insight into the aptamer-dependent fluorescence enhancement in *E. coli*. In regards to both reductive and oxidative sensing, cells displayed statistically significant fluorescence enhancement over 60 minutes of incubation with the target inorganic redox species. The degree of heterogeneity in fluorescence intensity, especially for 15- and 30-minute samples, supported the visual increase of brightness over time. Samples incubated with PyDSBz-DBrHBI (100 μM) and then exposed to exogenous Na_2S (2 mM) showed a progressive increase in cell populations with detectable intracellular fluorescence over the course of imaging (Figures 6B bottom and 6C). After 60 minutes of Na_2S treatment, the mean fluorescence intensity value was determined to be 105-fold higher than that at 0 minute (147.6 vs 1.4). The single cell fluorescence outputs were detected within 15 minutes upon addition of Na_2S, which then plateaued over 60 minutes (Figure 6C). We observed similar trends in *E. coli* incubated with MBBA-MFHBI (100 μM) and then exposed to H_2O_2 (100 μM) (Figures 6D bottom and 6E). The mean fluorescence intensity increased from 2.6 a.u. at 0 minute to 181.7 a.u. at 60 minutes following H_2O_2 addition. The single cell fluorescence intensities reached to a maximum (centered around 200 a.u.) within 30 minutes, while the overall mean fluorescence of the *E. coli* populations progressively increased over 60 minutes.

Conclusion

Interest in fluorescent light-up aptamer (FLAP)-based target detection is substantial given the ever-evolving needs in analyte biosensing, diagnostics, and environmental surveillance.[6–19, 66–69] The traditional target recognition, whether directly by the FLAP itself or through its conditional folding induced by a secondary aptamer domain,[20] entails the availability of an aptamer consensus sequence for each distinct target. Even though these approaches find biological use, repurposing a single aptamer to detect multiple and chemically diverse targets, especially inorganic and reactive molecules, has yet to be realized. Our study describes how small molecules can address these fundamental challenges. Guided by molecular docking (Figures 2, S1, and S2) and functional group reactivities in synthetic organic chemistry, we built a library of benzylidene imidazolinone compounds to screen for redox-responsive pre-ligands of the RNA aptamer Baby Spinach (Figure 3). Among those, PyDSBz-DBrHBI and MBBA-MFHBI showed favorable solubility, stability, and redox selectivity profiles. In addition, both pre-ligands displayed markedly inhibited fluorogenic binding to Baby Spinach (Figure 4), providing minimal background signal generation. Of note, the molecular docking approach presented here serves as a low-level computational support for pre-ligand designs. We used CH to substitute boron for the MBBA caging group, which deviates from the ideal pre-ligand structure.

The activity-based sensing platform using Baby Spinach and a defined pre-ligand exhibited significant levels of fluorescence enhancement in the presence of its respective inorganic target, H_2S/HS^- or H_2O_2 (Figure 5). Our small-molecule approach can be employed with other RNA aptamers. Specific examples we tested here include Broccoli and Squash. Both PyDSBz-DBrHBI and MBBA-MFHBI exhibited weak binding to these aptamers, yet they led to increased fluorescence upon treatment with the target redox species (Figures S8 and S9). Of note, the target sensitivities and rates of fluorescence generation are comparable to those of previously reported small-molecule fluorophores.[57–61] Further, the real-time sensing of redox molecules with aptamers could be achieved by optimizing pre-ligands to react more rapidly without compromising selectivity. This platform is also open to pre-ligands tailored to detect other reactive species (e.g., $O_2^{-\bullet}$,[70] Cu(I)[71]). Additional applications could involve pre-ligands for sensing broader classes of biological targets. Notably, 4-*O*-peptidyl benzylidene imidazolinones could enable the aptamer-based sensing of proteases, especially those overexpressed in cancer.

We demonstrated the implementation of aptamer-based redox sensing in *E. coli* through plasmid transfection followed by pre-ligand incubation, which conveniently transformed the bacteria into cell-based sensors (Figure 6). Key advantages of the described platform include that, unlike most stand-alone fluorophores, pre-ligands exhibit minimal background fluorescence, and the genetically encoded aptamer can allow for a consistent signal throughout the proliferating cell populations. Future directions in cell-based biosensing involve the expansion of organismal diversity beyond *E. coli*. We envision integrating the reported FLAP/pre-ligand system into eukaryotes, such as yeast and mammalian cells. The interaction between the aptamer and ligand is fairly strong (K_d or 950 nM for DBrHBI and 660 nM for MFHBI[72]), which can maintain a relatively stable complex inside the cell. Further optimization of the aptamer binding is required to reduce the impact of dynamic intracellular ligand concentrations caused by diffusion. Efforts to establish these platforms are currently ongoing in our lab.

This work demonstrates the potential of synthetic organic chemistry for advancing the applications of aptamers beyond their current capabilities in analyte sensing and synthetic biology.

Supporting Information

The authors have cited additional references within the Supporting Information.[73–76]

Acknowledgements

We thank Edward W. Castner, Advaitha Madireddy, Darrin York, Jia Sheng, George Giambasu, Alec Meacham, Robert Puhak, Kern Hast and Jonathan Hong for useful discussions. We acknowledge Magali Rhia L. Stone for guidance in microscopy sample preparation. We thank Xinyi (Cindy)

Miao for assistance in fluorescence quantification of *E. coli*. We thank Anuva Joshi and Serena Yee for assistance with in vitro transcription and gel electrophoresis. We acknowledge the Office of Advanced Research Computing (OARC) at Rutgers for providing access to the Amarel cluster. This work was supported by the US National Institutes of Health/National Institute of Biomedical Imaging and Bioengineering, Trailblazer Award (EB029548), the American Cancer Society, Institutional Research Grant Early Investigator Award, and the Rutgers Cancer Institute of New Jersey NCI Cancer Center Support Grant (P30CA072720), and Busch Biomedical Grant (to E.C.I.); and Steven A. Cox Scholarship for Cancer Research (to T.A. and L.W.).

Conflict of Interest

E.C.I. and T.A. are co-inventors in a patent application filed by Rutgers University on the subject of this work.

Data Availability Statement

The data that support the findings of this study are available from the corresponding author upon reasonable request.

Keywords: Aptamers · small-molecule ligand · cell-based biosensor · redox processes · synthetic biology

[1] C. Tuerk, L. Gold, *Science* **1990**, *249*, 505–510.
[2] A. D. Ellington, J. W. Szostak, *Nature* **1990**, *346*, 818–822.
[3] A. Roth, R. R. Breaker, *Annu. Rev. Biochem.* **2009**, *78*, 305–334.
[4] S. C. B. Gopinath, *Anal. Bioanal. Chem.* **2006**, *387*, 171–182.
[5] S. Neubacher, S. Hennig, *Angew. Chem. Int. Ed.* **2019**, *58*, 1266–1279.
[6] E. M. McConnell, J. Nguyen, Y. Li, *Front. Chem.* **2020**, *8*, 434.
[7] J. Gooch, B. Daniel, M. Parkin, N. Frascione, *TrAC Trends Anal. Chem.* **2017**, *94*, 150–160.
[8] X. C. Wang, S. C. Wilson, M. C. Hammond, *Nucleic Acids Res.* **2016**, *44*, e139–e139.
[9] T. Kato, I. Shimada, R. Kimura, M. Hyuga, *Chem. Commun.* **2016**, *52*, 4041–4044.
[10] P. Khan, L. M. Aufdembrink, A. E. Engelhart, *ACS Synth. Biol.* **2020**, *9*, 2861–2880.
[11] D. M. Kolpashchikov, A. A. Spelkov, *Angew. Chem. Int. Ed.* **2021**, *60*, 4988–4999.
[12] L. Wang, K. Hast, T. Aggarwal, M. Baci, J. Hong, E. C. Izgu, *Bioorg. Med. Chem.* **2022**, *69*, 116909.
[13] R. Wu, A. P. K. K. K. Mudiyanselage, F. Shafiei, B. Zhao, Y. Bagheri, Q. Yu, K. McAuliffe, K. Ren, M. You, *Angew. Chem. Int. Ed.* **2019**, *58*, 18271–18275.
[14] K. Ren, R. Wu, A. P. K. K. K. Mudiyanselage, Q. Yu, B. Zhao, Y. Xie, Y. Bagheri, Q. Tian, M. You, *J. Am. Chem. Soc.* **2020**, *142*, 2968–2974.
[15] M. Sunbul, J. Lackner, A. Martin, D. Englert, B. Hacene, F. Grün, K. Nienhaus, G. U. Nienhaus, A. Jäschke, *Nat. Biotechnol.* **2021**, *39*, 686–690.
[16] Z. Sun, R. Wu, B. Zhao, R. Zeinert, P. Chien, M. You, *Angew. Chem. Int. Ed.* **2021**, *60*, 24070–24074.
[17] D. Englert, E.-M. Burger, F. Grün, M. S. Verma, J. Lackner, M. Lampe, B. Bühler, J. Schokolowski, G. U. Nienhaus, A. Jäschke, M. Sunbul, *Nat. Commun.* **2023**, *14*, 3879.
[18] M. R. Dunn, C. M. McCloskey, P. Buckley, K. Rhea, J. C. Chaput, *J. Am. Chem. Soc.* **2020**, *142*, 7721–7724.
[19] A. Climent-Catala, T. E. Ouldridge, G.-B. V. Stan, W. Bae, *ACS Synth. Biol.* **2022**, *11*, 562–569.
[20] Y. Su, M. C. Hammond, *Curr. Opin. Biotechnol.* **2020**, *63*, 157–166.
[21] M. You, J. L. Litke, S. R. Jaffrey, *Proc. Nat. Acad. Sci.* **2015**, *112*, E2756–E2765.
[22] R. C. Spitale, D. Incarnato, *Nat. Rev. Genet.* **2023**, *24*, 178–196.
[23] L. R. Ganser, M. L. Kelly, D. Herschlag, H. M. Al-Hashimi, *Nat. Rev. Mol. Cell Biol.* **2019**, *20*, 474–489.
[24] Q. Hou, S. R. Jaffrey, *RNA Biol.* **2023**, *20*, 198–206.
[25] U. Förster, J. E. Weigand, P. Trojanowski, B. Suess, J. Wachtveitl, *Nucleic Acids Res.* **2012**, *40*, 1807–1817.
[26] J. S. Paige, K. Y. Wu, S. R. Jaffrey, *Science* **2011**, *333*, 642–646.
[27] K. D. Warner, M. C. Chen, W. Song, R. L. Strack, A. Thorn, S. R. Jaffrey, A. R. Ferré-D'Amaré, *Nat. Struct. Mol. Biol.* **2014**, *21*, 658–663.
[28] H. Huang, N. B. Suslov, N.-S. Li, S. A. Shelke, M. E. Evans, Y. Koldobskaya, P. A. Rice, J. A. Piccirilli, *Nat. Chem. Biol.* **2014**, *10*, 686–691.
[29] R. L. Strack, M. D. Disney, S. R. Jaffrey, *Nat. Methods* **2013**, *10*, 1219–1224.
[30] B. Olas, *Adv. Clin. Chem.* **2016**, *78*, 187–196.
[31] H. Kimura, *Biochem. Biophys. Res. Commun.* **2000**, *267*, 129–133.
[32] Y. Han, J. Qin, X. Chang, Z. Yang, D. Bu, J. Du, *Neurosci. Res.* **2005**, *53*, 216–219.
[33] W.-H. Sun, F. Liu, Y. Chen, Y.-C. Zhu, *Biochem. Biophys. Res. Commun.* **2012**, *421*, 164–169.
[34] Y. Kimura, Y.-I. Goto, H. Kimura, *Antioxid. Redox Signaling* **2010**, *12*, 1–13.
[35] D. J. Lefer, *Proc. Nat. Acad. Sci.* **2007**, *104*, 17907–17908.
[36] D. J. Polhemus, D. J. Lefer, *Circ. Res.* **2014**, *114*, 730–737.
[37] J. C. Mathai, A. Missner, P. Kügler, S. M. Saparov, M. L. Zeidel, J. K. Lee, P. Pohl, *Proc. Nat. Acad. Sci.* **2009**, *106*, 16633–16638.
[38] B. D'Autréaux, M. B. Toledano, *Nat. Rev. Mol. Cell Biol.* **2007**, *8*, 813–824.
[39] H. Sies, D. P. Jones, *Nat. Rev. Mol. Cell Biol.* **2020**, *21*, 363–383.
[40] H. Sies, *J. Biol. Chem.* **2014**, *289*, 8735–8741.
[41] C. Lennicke, J. Rahn, R. Lichtenfels, L. A. Wessjohann, B. Seliger, *Cell Commun. Signaling* **2015**, *13*, 39.
[42] J. V. Cordeiro, A. Jacinto, *Nat. Rev. Mol. Cell Biol.* **2013**, *14*, 249–262.
[43] E. C. Cheung, K. H. Vousden, *Nat. Rev. Cancer* **2022**, *22*, 280–297.
[44] G. P. Bienert, A. L. B. Møller, K. A. Kristiansen, A. Schulz, I. M. Møller, J. K. Schjoerring, T. P. Jahn, *J. Biol. Chem.* **2007**, *282*, 1183–1192.
[45] G. P. Bienert, B. Desguin, F. Chaumont, P. Hols, *Biochem. J.* **2013**, *454*, 559–570.
[46] O. Trott, A. J. Olson, *J. Comput. Chem.* **2010**, *31*, 455–461.
[47] J. Eberhardt, D. Santos-Martins, A. F. Tillack, S. Forli, *J. Chem. Inf. Model.* **2021**, *61*, 3891–3898.
[48] M. Su, Q. Yang, Y. Du, G. Feng, Z. Liu, Y. Li, R. Wang, *J. Chem. Inf. Model.* **2019**, *59*, 895–913.
[49] Z. Wang, Y. Li, Q. Zhang, C. Jing, Y. Jiang, T. Yang, T. Han, F. Xiong, *Spectrochim. Acta Part A: Mol. Biomol. Spectrosc.* **2023**, *293*, 122428.
[50] V. S. Lin, W. Chen, M. Xian, C. J. Chang, *Chem. Soc. Rev.* **2014**, *44*, 4596–4618.

[51] B. Peng, W. Chen, C. Liu, E. W. Rosser, A. Pacheco, Y. Zhao, H. C. Aguilar, M. Xian, *Chem. A Eur. J.* **2014**, *20*, 1010–1016.
[52] A. R. Lippert, G. C. V. de Bittner, C. J. Chang, *Acc. Chem. Res.* **2011**, *44*, 793–804.
[53] E. Cuevasanta, M. Lange, J. Bonanata, E. L. Coitiño, G. Ferrer-Sueta, M. R. Filipovic, B. Alvarez, *J. Biol. Chem.* **2015**, *290*, 26866–26880.
[54] A. K. Yadav, Z. Zhao, Y. Weng, S. H. Gardner, C. J. Brady, O. D. P. Peguero, J. Chan, *J. Am. Chem. Soc.* **2023**, DOI 10.1021/jacs.2c12984.
[55] A. Papapetropoulos, A. Pyriochou, Z. Altaany, G. Yang, A. Marazioti, Z. Zhou, M. G. Jeschke, L. K. Branski, D. N. Herndon, R. Wang, C. Szabó, *Proc National Acad Sci* **2009**, *106*, 21972–21977.
[56] Q. Li, J. R. Lancaster, *Nitric Oxide* **2013**, *35*, 21–34.
[57] M. Pose, K. M. Dillon, A. Denicola, B. Alvarez, J. B. Matson, M. N. Möller, E. Cuevasanta, *J. Biol. Chem.* **2022**, *298*, 102402.
[58] S. Peng, T. Zhong, T. Guo, D. Shu, D. Meng, H. Liu, D. Guo, *N.J. Chem.* **2018**, *42*, 5185–5192.
[59] H. Chen, X. Wu, S. Yang, H. Tian, Y. Liu, B. Sun, *J. Anal. Methods Chem.* **2019**, *2019*, 2173671.
[60] H. R. Bolland, E. M. Hammond, A. C. Sedgwick, *Chem. Commun.* **2022**, *58*, 10699–10702.
[61] Y. Zuo, Y. Jiao, C. Ma, C. Duan, *Molecules* **2021**, *26*, 3352.
[62] G. S. Filonov, J. D. Moon, N. Svensen, S. R. Jaffrey, *J. Am. Chem. Soc.* **2014**, *136*, 16299–16308.
[63] L. Truong, H. Kooshapur, S. K. Dey, X. Li, N. Tjandra, S. R. Jaffrey, A. R. Ferré-D'Amaré, *Nat. Chem. Biol.* **2022**, *18*, 191–198.
[64] A. S. Khalil, J. J. Collins, *Nat. Rev. Genet.* **2010**, *11*, 367–379.
[65] D. M. Shechner, E. Hacisuleyman, S. T. Younger, J. L. Rinn, *Nat. Methods* **2015**, *12*, 664–670.
[66] R. P. Connelly, P. F. Madalozzo, J. E. Mordeson, A. D. Pratt, Y. V. Gerasimova, *Chem. Commun.* **2021**, *57*, 3672–3675.
[67] C. H. Park, I. A. P. Thompson, S. S. Newman, L. A. Hein, X. Lian, K. X. Fu, J. Pan, M. Eisenstein, H. T. Soh, *Adv. Mater.* **2024**, *36*, e2306704.
[68] J. Canoura, O. Alkhamis, M. Venzke, P. T. Ly, Y. Xiao, *JACS Au* **2024**, *4*, 1059–1072.
[69] O. Alkhamis, J. Canoura, Y. Wu, N. A. Emmons, Y. Wang, K. M. Honeywell, K. W. Plaxco, T. E. Kippin, Y. Xiao, *J. Am. Chem. Soc.* **2024**, *146*, 3230–3240.
[70] K. Xu, X. Liu, B. Tang, G. Yang, Y. Yang, L. An, *Chem. A Eur. J.* **2007**, *13*, 1411–1416.
[71] C. Y.-S. Chung, J. M. Posimo, S. Lee, T. Tsang, J. M. Davis, D. C. Brady, C. J. Chang, *Proc. Nat. Acad. Sci.* **2019**, *116*, 18285–18294.
[72] W. Song, R. L. Strack, N. Svensen, S. R. Jaffrey, *J. Am. Chem. Soc.* **2014**, *136*, 1198–1201.
[73] B. Gutierrez, T. Aggarwal, H. Erguven, M. R. L. Stone, C. Guo, A. Bellomo, E. Abramova, E. R. Stevenson, D. L. Laskin, A. J. Gow, E. C. Izgu, *iScience* **2023**, *26*, 108567.
[74] H. Erguven, L. Wang, B. Gutierrez, A. H. Beaven, A. J. Sodt, E. C. Izgu, *JACS Au* **2024**, *4*, 1841–1853.
[75] Gaussian 09, Revision D.01, M. J. Frisch, G. W. Trucks, H. B. Schlegel, G. E. Scuseria, M. A. Robb, J. R. Cheeseman, G. Scalmani, V. Barone, B. Mennucci, G. A. Petersson, H. Nakatsuji, M. Caricato, X. Li, H. P. Hratchian, A. F. Izmaylov, J. Bloino, G. Zheng, J. L. Sonnenberg, M. Hada, M. Ehara, K. Toyota, R. Fukuda, J. Hasegawa, M. Ishida, T. Nakajima, Y. Honda, O. Kitao, H. Nakai, T. Vreven, J. A. Montgomery, Jr., J. E. Peralta, F. Ogliaro, M. Bearpark, J. J. Heyd, E. Brothers, K. N. Kudin, V. N. Staroverov, R. Kobayashi, J. Normand, K. Raghavachari, A. Rendell, J. C. Burant, S. S. Iyengar, J. Tomasi, M. Cossi, N. Rega, J. M. Millam, M. Klene, J. E. Knox, J. B. Cross, V. Bakken, C. Adamo, J. Jaramillo, R. Gomperts, R. E. Stratmann, O. Yazyev, A. J. Austin, R. Cammi, C. Pomelli, J. W. Ochterski, R. L. Martin, K. Morokuma, V. G. Zakrzewski, G. A. Voth, P. Salvador, J. J. Dannenberg, S. Dapprich, A. D. Daniels, Ö. Farkas, J. B. Foresman, J. V. Ortiz, J. Cioslowski, and D. J. Fox, Gaussian, Inc., Wallingford CT, 2009.
[76] G. M. Morris, R. Huey, W. Lindstrom, M. F. Sanner, R. K. Belew, D. S. Goodsell, A. J. Olson, *J. Comput. Chem.* **2009**, *30*, 2785–2791.

Manuscript received: November 11, 2024
Accepted manuscript online: December 12, 2024
Version of record online: December 20, 2024